



F3

**Faculty of Electrical Engineering
Department of Cybernetics**

Bachelor's Thesis

Fusion of UWB-Based Distance Sensors with a Visual Relative Localization System

Vít Petřík

**Supervisor: Ing. Viktor Walter
Field of study: Cybernetics and robotics
May 2023**

I. Personal and study details

Student's name: **Petřík Vít**

Personal ID number: **499246**

Faculty / Institute: **Faculty of Electrical Engineering**

Department / Institute: **Department of Cybernetics**

Study program: **Cybernetics and Robotics**

II. Bachelor's thesis details

Bachelor's thesis title in English:

Fusion of UWB-Based Distance Sensors with a Visual Relative Localization System

Bachelor's thesis title in Czech:

Fúze senzoru vzdálenosti na báze UWB se systémem vizuální relativní lokalizace

Guidelines:

Range sensors based on the UWB (Ultra-wideband) signal technology enable robust wireless measurement of relative distance between two devices. This property complements the drawbacks of relative localization based on computer vision, such as the UVDAR system used by the MRS group, namely their reduced precision in terms of distance estimation. Compared to UWB sensors however, computer vision methods make it possible to estimate the relative bearing of a target.

If used together, the two sensor types can enable a more precise relative localization of flying Unmanned Aerial Vehicles (UAVs) than if each was used separately.

The goal of this thesis is to develop a system for fusion of the output data from the two aforementioned sensor types, and to implement this system in the Robot Operating System (ROS).

The system should optionally also be tested on real flying UAV.

Bibliography / sources:

- [1] V. Walter, N. Staub, A. Franchi and M. Saska. UVDAR System for Visual Relative Localization With Application to Leader–Follower Formations of Multirotor UAVs. IEEE Robotics and Automation Letters 4(3):2637-2644, July 2019.
- [2] Y. Shimizu and Y. Sanada, "Accuracy of relative distance measurement with ultra wideband system," IEEE Conference on Ultra Wideband Systems and Technologies, 2003, 2003, pp. 374-378, doi: 10.1109/UWBST.2003.1267867.
- [3] Stanford Artificial Intelligence Laboratory et al. (2018). Robotic Operating System. Retrieved from <https://www.ros.org>

Name and workplace of bachelor's thesis supervisor:

Ing. Viktor Walter Multi-robot Systems FEE

Name and workplace of second bachelor's thesis supervisor or consultant:

Date of bachelor's thesis assignment: **20.02.2023** Deadline for bachelor thesis submission: _____

Assignment valid until: **22.09.2024**

Ing. Viktor Walter
Supervisor's signature

prof. Ing. Tomáš Svoboda, Ph.D.
Head of department's signature

prof. Mgr. Petr Páta, Ph.D.
Dean's signature

III. Assignment receipt

The student acknowledges that the bachelor's thesis is an individual work. The student must produce his thesis without the assistance of others, with the exception of provided consultations. Within the bachelor's thesis, the author must state the names of consultants and include a list of references.

Date of assignment receipt

Student's signature

Acknowledgements

Děkuji ČVUT, že mi je tak dobrou *alma mater*.

Declaration

I declare that the presented work was developed independently and that I have listed all sources of information used within it in accordance with the methodical instructions for observing the ethical principles in the preparation of university theses. V Praze, 10. May 2023

Abstract

For the operation of multi-robot systems, it is crucial that each robot possesses information about the whole system. This information could be GNSS coordinates shared through multiple robots. This approach, however falls apart when the system needs to operate indoors. A popular solution for such a problem is to employ visual relative localizations.

This thesis discusses possible paths to improve measurements from relative visual localizations. A proposed solution for this task is a sensor based on Ultra-wideband technology. As our experiments show, the solution offers high precision and low latency localization of multiple robots.

Keywords: word, key

Supervisor: Ing. Viktor Walter

Abstrakt

TODO

Klíčová slova: slovo, klíč

Překlad názvu: Fúze senzoru vzdálenosti na báze UWB se systémem vizuální relativní lokalizace

Contents

1 Introduction	1	6.0.1 Line segment test	23
2 Ultra-violet Detection and Ranging	3	6.0.2 Circular trajectory	23
3 Ultra-wide band	5	6.0.3 Leader follower algorithm ...	24
3.1 MAC layer	6	6.1 Results	24
3.2 Physical Layer.....	7		
PPDU format	8		
3.2.1 Symbol structure	9		
3.3 Ranging techniques	12		
Time Difference of Arrival	12		
Two way ranging	13		
4 Kalman filters	17		
4.1 Linear Kalman filter	18		
4.2 Unscented Kalman filter	19		
5 Implementation on MAV	21		
6 Simulations and real-world experiments	23		
7 Conclusion	27		
Bibliography	29		

Figures

2.1 Image from UV camera.	4	6.3 Transfer characteristic of UWB	25
2.2 UVDAR processing data flow. [12]	4	6.4 Transfer characteristic of UWB	26
3.1 OSI-ISO network model.	6		
3.2 Data flow according to [1].	7		
3.3 PPDU encoding process [1].	9		
3.4 SHR field structure. [3]	9		
3.5 PHR field structure. [3]	10		
3.6 Example of BPM-BPSK modulation,	10		
3.7 Symbol stucture. [3]	11		
3.8 Reference pulse of UWB radio.	12		
3.9 Two way ranging with two round trips.	14		
4.1 Comparsion between sampling, EKF and sigma points. [7]	19		
6.1 Holybro X500	24		
6.2 Transfer characteristic of UWB	25		

Tables

3.1 MAC frame format.	7
3.2 Reference pulse duration for each channel. [1]	11

Chapter 1

Introduction

In recent years, the use of unmanned aerial vehicles (UAVs) has been rapidly growing due to their versatility and wide range of applications, from aerial photography and surveillance to delivery services¹ and search and rescue operations [8]. The problem of relative localization in UAV swarms is a critical challenge for enabling cooperative behavior and avoiding collisions.

To address this problem, a novel system is proposed in this thesis that combines computer vision and ultra-wideband (UWB) technology for direction and range measurements, respectively. By fusing these measurements using a Kalman filter, the relative positions and orientations of UAVs can be estimated with high accuracy, even in GNSS-denied environments such as undergrounds, buildings or caves [8]. This approach has a significant advantage over existing methods, which often rely on GNSS [10] or motion capture² and are therefore limited in their ability to operate in challenging environments or without additional infrastructure onsite.

The research question for this thesis is: How can an effective relative localization system for UAV swarms be designed and implemented using computer vision and UWB technology, and how well does it perform in real-world scenarios? Firstly, a review of the existing literature on relative localization and multi-robot systems will be conducted. Secondly, the proposed system and its key components, including the computer vision algorithms for direction estimation and the UWB hardware for range measurement, will be presented. Finally, the performance of the system will be evaluated through a series of experiments in both simulated and real-world environments and compared with existing approaches.

By developing and testing this system, a contribution will be made to the

¹Blood and packages delivery <https://www.flyzipline.com>

²Motion capture OptiTrack <https://optitrack.com>

1. Introduction

growing body of research on multi-robot systems and pave the way for new applications of UAV swarms in challenging environments.

Chapter 2

Ultra-violet Detection and Ranging

The Ultra-violet Direction and Ranging (UVDAR) is a system for relative localization based on computer vision. The system was developed by the Multi-robot system group at CTU [13]. It consists of two parts, active UV LED markers and industrial grade camera with UV bandpass filter and fish-eye lens. This allows the system to exactly recognize active markers from the background and work even in a pitch-black environment. This effect can be seen in image 2.1.

2. Ultra-violet Detection and Ranging



Figure 2.1: Image from UV camera.

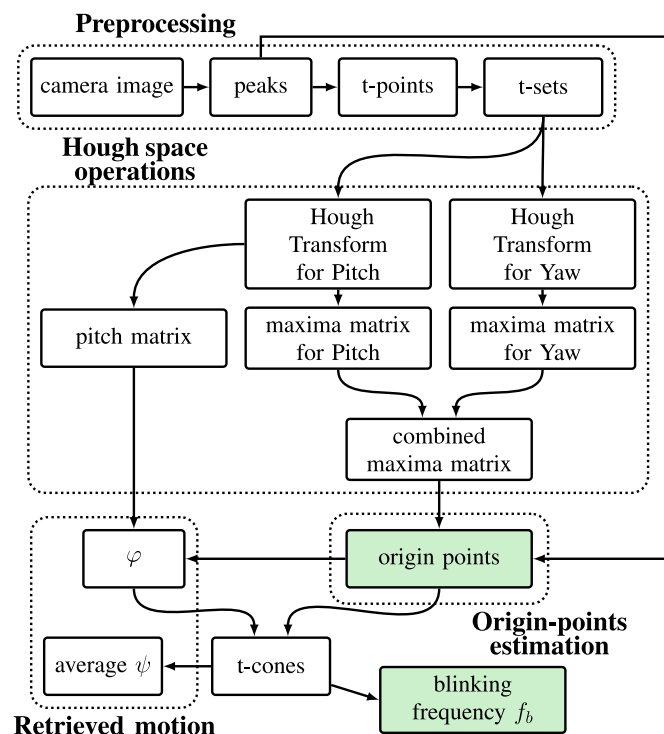


Figure 2.2: UVDAR processing data flow. [12]

Chapter 3

Ultra-wide band

The following chapter will introduce ultra-wide band by means of IEEE 802.15.4 [1]. There is another definition by Federal Communications Commission (FCC), however it will not be discussed in this thesis.

To fully understand what ultra-wide band means it is necessary to define what bandwidth means by equation 3.1 and what center frequency means by equation 3.2.

$$\text{bandwidth}_{-3\text{dB}} = f_{max} - f_{min} \quad (3.1)$$

$$f_{center} = \frac{f_{max} - f_{min}}{2} = f_{0db} \quad (3.2)$$

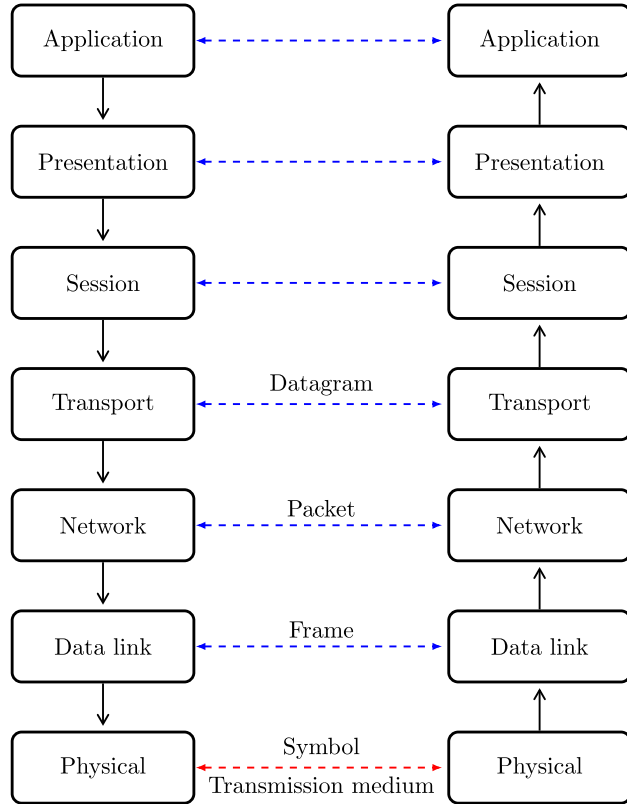
The ultra-wide band radio use bandwidth of 500 Mhz and more. This fact provides UWB with its unique ranging capabilities. The *IEEE 802.15.4 Low-Rate Wireless Personal Area Networks* [1] specifies physical and data link layers from the ISO-OSI network model 3.1.

Today UWB is mainly used in consumer electronics¹ or in a manufacturing plant to track assets, ground vehicles and people²³.

¹Apple AirTag <https://www.apple.com/airtag/>

²Siemens RTLS <https://www.siemens.com/global/en/products/automation/industrial-identification/simatic-rtls.html/>

³Sewio real-time location system <https://www.sewio.net/>

**Figure 3.1:** OSI-ISO network model.

3.1 MAC layer

IEEE 802.15.4 describes the MAC layer for low-rate wireless personal networks, including UWB. The MAC layer is responsible for coordinating access to the shared wireless channel, managing network associations and disassociations, and providing security and reliability features. The MAC layer inserts a MAC header and a MAC footer before and after a network-layer frame, respectively. The MAC header contains information such as frame type, source and destination addresses, sequence number, and security parameters. The MAC footer contains a CRC check. The IEEE 802.15.4 MAC layer supports two modes of operation: beacon-enabled and non-beacon-enabled. In beacon-enabled mode, a coordinator device periodically broadcasts beacons to synchronize the devices in its network and allocate contention-free periods for data transmission. In non-beacon-enabled mode, devices use a slotted or unslotted carrier sense multiple access with collision avoidance (CSMA-CA)

Bytes: 2	1	0/2	0/2/8	0/2	0/2/8	0/5/6/10/14	variable	2
Frame Control	Sequence Number	Destination PAN Identifier	Destination Address	Source PAN Identifier	Source Address	Auxiliary Security Header	Frame Payload	FCS
		Addressing fields						
MHR							MAC Payload	MFR

Table 3.1: MAC frame format.

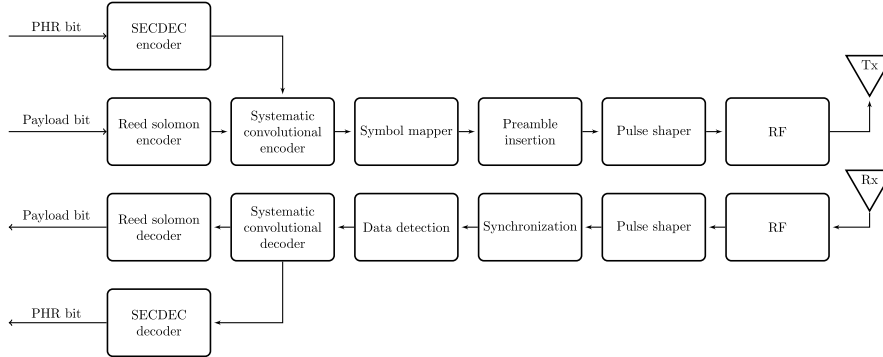


Figure 3.2: Data flow according to [1].

mechanism to access the channel. The exact layout of MAC frame format is described in Table 3.1.

3.2 Physical Layer

The physical (PHY) layer of UWB was described in IEEE 802.15.4-2011 [1] as UWB PHY. Later in IEEE 802.15.4-2015 [3] the PHY was named as High repetition pulse (HRP) UWB PHY. This decision was made due to the introduction of Low repetition pulse (LRP) UWB PHY. Only the HRP UWB PHY will be discussed. The standard defines three operation bands:

- sub-gigahertz band consisting of single a channel spectrum from 249.6 MHz to 749.6 MHz.
- Low band with spectrum from 3.1 GHz to 4.8 GHz.
- High band with spectrum from 6 GHz to 10.6 GHz.

It uses an impulse radio signaling scheme with band-limited pulses and supports high data rates and precision ranging applications. It also uses

3. Ultra-wide band

a combination of burst position modulation (BPM) and binary phase-shift keying (BPSK) to modulate symbols. The overview of the physical layer is expressed in figure 3.2.

■ PPDU format

Each physical layer protocol data unit (PPDU) consists of a preamble, PHY header, and the data itself. The process of encoding the whole PPDU can be seen in figure 3.3.

Reed-Solomon encoding is used to encode the physical service data unit (PSDU) of the HRP UWB PHY. It adds redundant symbols to the original message symbols to form a codeword that can be decoded using polynomial interpolation or factorization techniques. Reed-Solomon encoding improves the error-correction performance of the HRP UWB PHY and enables it to handle burst errors or random errors that may occur in the wireless channel⁴.

Convolutional encoding is used to encode the PSDU of the HRP UWB PHY after Reed-Solomon encoding. It uses a finite state machine with memory cells to generate output bits based on the current and previous input bits. It adds parity bits to the original information bits to form a codeword that can be decoded using Viterbi algorithm or other sequential decoding techniques. Convolutional encoding improves the error-correction performance of the HRP UWB PHY and enables it to handle noisy or fading channels.

A preamble in HRP UWB PHY is a sequence of known bits sent at the beginning of each frame. It is used for frame synchronization, channel estimation, and ranging measurements. It consists of two parts: a synchronization header (SHR) 3.4 and a physical layer header (PHR) 3.5.

The SHR contains a preamble symbol (SYNC) and a start-of-frame delimiter (SFD). The SFD is a fixed sequence of pulses that indicates the start of a frame. The PS is a burst of UWB pulses that can be modulated by burst position modulation (BPM) or binary phase-shift keying (BPSK). The preamble symbol repetitions (PSR) define the number of repeated sequences, ranging from 16 to 4,096 repetitions.

⁴Mathworks HRP UWB IEEE 802.15.4a/z Waveform Generation
<https://www.mathworks.com/help/comm/ug/hrp-uwb-ieee-802.15.4az-waveform-generation.html>

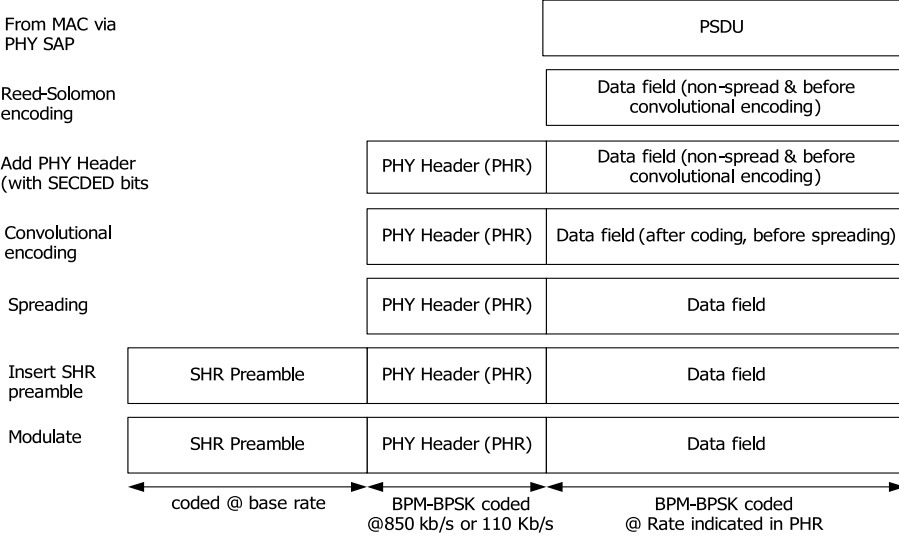


Figure 3.3: PPDU encoding process [1].

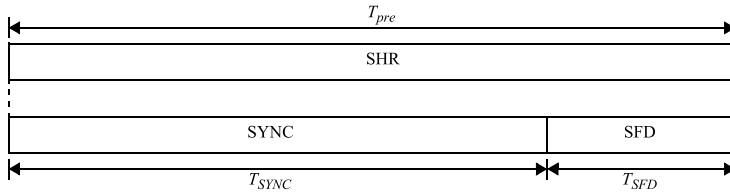


Figure 3.4: SHR field structure. [3]

The PHR contains information about the data to be received, including the length of the data and the data rate used to transmit the data. It also contains additional information elements to facilitate ranging information exchange

3.2.1 Symbol structure

A symbol 3.7 is the basic unit of information in HWP UWB PHY. It consists of a short burst of UWB pulses that lasts for 2 ns and occupies a bandwidth of 0.5-1.3 GHz. The burst can be placed in one of the two possible burst intervals, and its phase can be inverted or not. These two choices allow each symbol to carry two bits of information using burst position modulation (BPM) and binary phase-shift keying (BPSK), a example of the modulation can be found in figure 3.6.

3. Ultra-wide band

Bits: 0–1	2–8	9	10	11–12	13–18
Data Rate	Frame Length	Ranging	Reserved	Preamble Duration	SECDED

Figure 3.5: PHR field structure. [3]

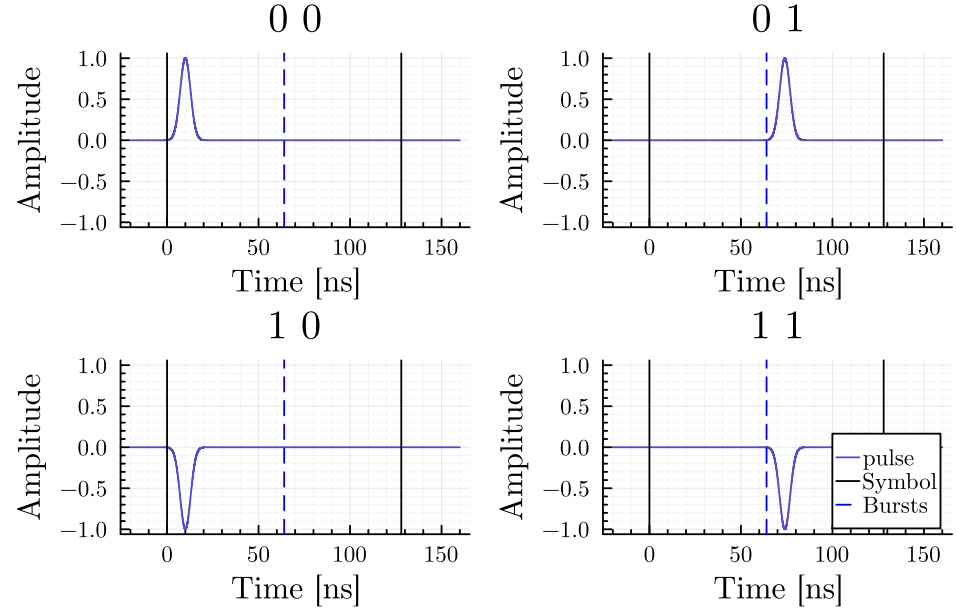


Figure 3.6: Example of BPM-BPSK modulation,

Burst hopping position is a parameter that determines the time position of the UWB pulses within a burst interval. Scrambling code is a pseudo-random sequence that is applied to the data bits before modulation. It is used to randomize the data bits and reduce the peak-to-average power ratio (PAPR) of the UWB pulses.

IEEE defines the reference pulse as a root-raised cosine pulse with roll-off factor $\beta = 0.5$ 3.3.

$$r(t) = \frac{4\beta}{\pi\sqrt{T_p}} \frac{\cos[(1+\beta)\pi t/T_p] + \frac{\sin[(1-\beta)\pi t/T_p]}{4\beta(t/T_p)}}{1 - (4\beta t/T_p)^2} \quad (3.3)$$

Parameter T_p stands for duration of the pulse. The duration is defined for each channel by table 3.2.

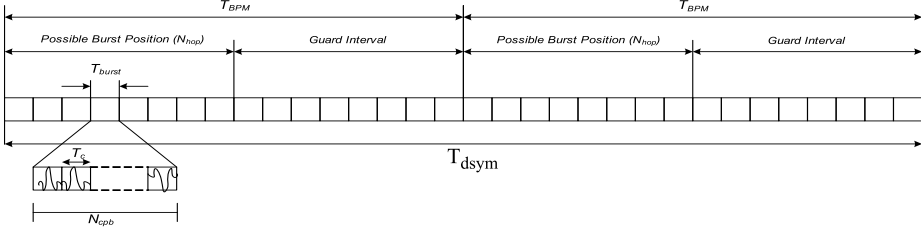


Figure 3.7: Symbol structure. [3]

Channel number	Pulse duration T_p (ns)	Main lobe width T_w (ns)
{0:3, 5:6, 8:10, 12:14}	2.00	0.5
7	0.92	0.2
{4, 11}	0.75	0.2
15	0.74	0.2

Table 3.2: Reference pulse duration for each channel. [1]

Figure 3.8 further illustrates a waveform of the pulse. However an actual hardware system cannot fully realize the shape of the reference pulse. Therefore IEEE 802.15.4 constrains transmitted pulse $p(t)$ by a cross-correlation function 3.4.

$$\phi(\tau) = \frac{1}{\sqrt{E_r E_p}} \operatorname{Re} \int_{-\infty}^{\infty} r(t)p(t - \tau)dt \quad (3.4)$$

Where:

E_r = energy of $r(t)$

E_p = energy of $p(t)$

For PHY to be IEEE compliant the main lobe of the transmitted pulse must have a magnitude of cross correlation $|\phi(\tau)|$ at least 0.8, and the magnitude of sidelobes must not be greater than 0.3.

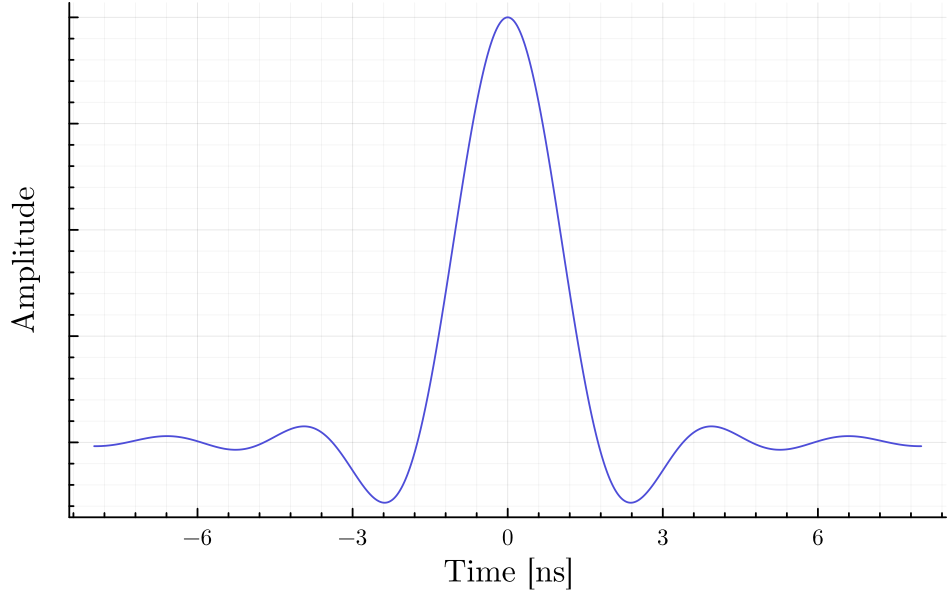


Figure 3.8: Reference pulse of UWB radio.

3.3 Ranging techniques

Time Difference of Arrival

Time difference of arrival (TDOA) position estimation is a technique that uses the difference in the arrival times of UWB signals at multiple receivers to estimate the position of a transmitter.

TDOA position estimation requires at least four receivers for 3D localization and one transmitter. The receivers measure the time of arrival (TOA) of the UWB signals. The TOA measurements are then used to calculate the TDOA values between different pairs of receivers [16].

To estimate the position of the transmitter system of equations 3.5 is solved [6]. For

$$\sqrt{\mathbf{x}_r^T \hat{\mathbf{x}}} - \sqrt{\mathbf{x}_i^T \hat{\mathbf{x}}} = c(t_r - t_i) \quad (3.5)$$

Where:

- $\hat{\mathbf{x}}$ = estimated position of the transmitter.
- \mathbf{x}_r = Position of the reference receiver.
- \mathbf{x}_i = Position of receiver i .
- t_r = Time of arrival for the reference receiver.
- t_i = Time of arrival for the receiver i .
- c = Speed of light.

The main challenge for implementing TDoA is synchronizing the clock across all receivers [15].

The TDoA system can be used in a variety of applications, such as indoor positioning, tracking of vehicles or people, and asset tracking. The accuracy of the TDoA system depends on the number and placement of the UWB sensors and the timing resolution of the system.

■ Two way ranging

Two-way ranging (TWR) is a technique used by UWB systems to estimate the distance between two devices. TWR requires two-way communication between two devices, where one device sends a signal to another device and waits for a response, as shown in figure 3.9. The time difference between the transmission and reception of the signal is used to calculate the distance between the two devices.

Single-sided two-way ranging (SS-TWR) is a technique where only one device sends a signal and waits for a response from another device. The time difference between the transmission and reception of the signal is used to calculate the distance between the two devices.

$$\text{TOF} = \frac{R_a - D_b}{2}$$

Where:

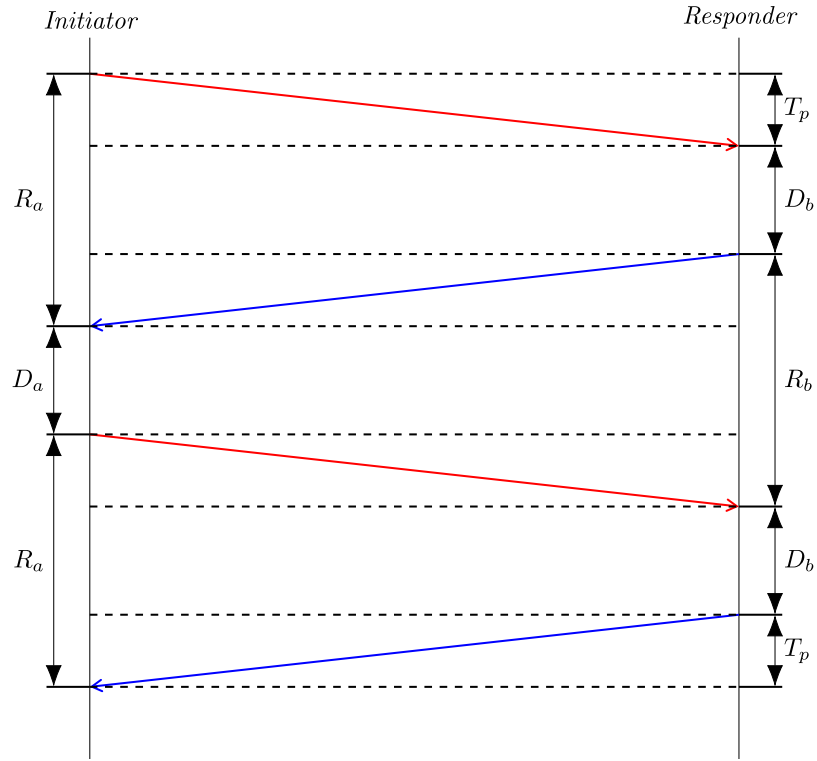


Figure 3.9: Two way ranging with two round trips.

TOF = Time of flight.

R_a = Time of round trip

D_b = Response delay.

Double-sided two-way ranging (DS-TWR) is a technique where both devices send signals and wait for responses from each other. The time difference between the transmission and reception of signals from both devices is used to calculate the distance between them.

$$\text{TOF} = \frac{R_a R_b - D_a D_b}{R_a + D_a + R_b + D_b}$$

DS-TWR's main advantage is its ability to compensate for the effect of clock drift [2]. Clock drift refers to several related phenomena where a clock does not run at exactly the same rate as a reference clock. That is, after some time the clock “drifts apart” or gradually desynchronizes from the other clock. All clocks are subject to drift, causing eventual divergence unless resynchronized. Clock drift can be caused by many factors, such as temperature changes, aging of components, and power supply voltage changes [2].

Chapter 4

Kalman filters

Kalman filters are a powerful mathematical technique used for estimating the state of a system from noisy measurements. Originally developed by Rudolf Kalman in 1960 [4], Kalman filters have become widely used in a variety of fields, including engineering, finance, and robotics. The Kalman filter is an optimal estimator, meaning that it provides the best estimate of the system state given the available measurements and knowledge of the system dynamics. The filter uses a mathematical model of the system, known as a state-space model, to predict the evolution of the system over time and to correct for measurement errors. The Kalman filter is particularly useful in applications where measurements are noisy or incomplete, or where the system dynamics are complex or difficult to model. In this way, the Kalman filter is an essential tool for many real-world applications that require accurate state estimation and control.

The algorithm involves two steps: prediction and update. The prediction step uses the previous state estimate and the motion model of the system to predict the current state estimate and its uncertainty. The update step uses the current measurement and the measurement model of the system to correct the predicted state estimate and its uncertainty using a weighted average. The weight is determined by the Kalman gain, which balances the trust between the prediction and the measurement. The Kalman gain is computed based on the covariance matrices of the prediction error and the measurement error. The prediction and update steps are performed recursively for each new measurement.

The linear kalman filter assumes that the system and the measurement models are linear and can be represented by matrices. The extended kalman filter extends the linear kalman filter to handle nonlinear systems by linearizing them around the current estimate using Taylor series expansion. The unscented kalman filter improves the extended kalman filter by using a set of sigma points to capture the mean and covariance of the nonlinear system

without requiring linearization or Jacobian matrices [5] [9]. The unscented kalman filter is more accurate and robust than the extended kalman filter, especially for highly nonlinear systems [9] [14].

4.1 Linear Kalman filter

A linear Kalman filter is a recursive algorithm that uses the Bode-Shannon representation of random processes and the state-transition method of analysis of dynamic systems to estimate the state of a system from noisy measurements. It assumes that the system and the measurements are linear and Gaussian, meaning that they can be expressed as matrix operations with additive noise. The algorithm consists of two steps: prediction and correction. In the prediction step 4.1, the algorithm uses a state transition matrix to project the current state and its covariance matrix to the next time step.

$$\begin{aligned}\hat{\mathbf{x}} &= \mathbf{F}\mathbf{x} + \mathbf{B}\mathbf{u} \\ \hat{\mathbf{P}} &= \mathbf{F}\mathbf{P}\mathbf{F}^T + \mathbf{Q}\end{aligned}\tag{4.1}$$

Where:

$\hat{\mathbf{x}}, \hat{\mathbf{P}}$ = State mean and covariance

\mathbf{F} = Transition matrix

\mathbf{Q} = Process matrix

\mathbf{B}, \mathbf{u} = Input to the system

In the correction step 4.2, the algorithm uses a measurement matrix to update the predicted state and its covariance matrix with the new measurement. The algorithm optimizes the estimation by minimizing the mean squared error between the true state and the estimated state [4].

$$\begin{aligned}\mathbf{y} &= \mathbf{z} - \mathbf{H}\mathbf{x} \\ \mathbf{K} &= \mathbf{P}\mathbf{H}^T(\mathbf{H}\mathbf{P}\mathbf{H}^T + \mathbf{R})^{-1} \\ \hat{\mathbf{x}} &= \mathbf{x} + \mathbf{K}\mathbf{y} \\ \hat{\mathbf{P}} &= (\mathbf{I} - \mathbf{K}\mathbf{H})\mathbf{P}\end{aligned}\tag{4.2}$$

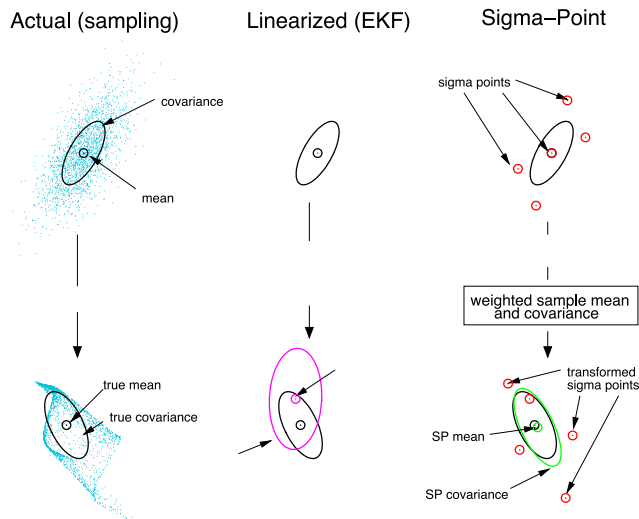


Figure 4.1: Comparsion between sampling, EKF and sigma points. [7]

Where:

\mathbf{z}, \mathbf{R} = Measurement and covariance

\mathbf{H} = Measurement function

4.2 Unscented Kalman filter

The unscented Kalman filter (UKF) is a technique for nonlinear estimation that uses a deterministic sampling approach to propagate a Gaussian random variable through the system dynamics [14]. The UKF employs the unscented transformation (UT), which generates a set of sample points that capture the mean and covariance of the original distribution.

The unscented transform is a technique for approximating the outcome of applying a nonlinear function to a probability distribution that is described by a mean and a covariance matrix. It does this by choosing a set of points, known as sigma points Figure 4.1.

Merwe describes generating the sigma points in his dissertation thesis [7].

4. Kalman filters

The sigma points \mathcal{X}_i as well as weights ω_i for each point are calculated using equation 4.3. The weights ω_i must follow equation $\sum_{i=0}^{2L} \omega_i = 1$.

$$\begin{aligned}\mathcal{X}_0 &= \bar{x} & \omega_0 &= \frac{\kappa}{L + \kappa} & i &= 0 \\ \mathcal{X}_i &= \bar{x} + \left(\sqrt{(L + \kappa) \mathbf{P}_{\mathbf{x}}} \right)_i & \omega_i &= \frac{1}{2(L + \kappa)} & i &= 1, \dots, L \\ \mathcal{X}_{i+L} &= \bar{x} - \left(\sqrt{(L + \kappa) \mathbf{P}_{\mathbf{x}}} \right)_i & \omega_i &= \frac{1}{2(L + \kappa)} & i &= L + 1, \dots, 2L\end{aligned}\quad (4.3)$$

Where:

$\hat{\mathbf{x}}, \mathbf{P}_{\mathbf{x}}$ = State vector and covariance

L = Dimension of state vector

κ = Scaling factor

The UKF has been shown to achieve higher accuracy and robustness than the extended Kalman filter (EKF) for various nonlinear estimation problems, such as state estimation, parameter estimation, and dual estimation [14].



Chapter 5

Implementation on MAV

Chapter 6

Simulations and real-world experiments

A series of experiments have been conducted to evaluate the performance of the proposed measurement system. Experiments took place at Temešvár and Císařský ostrov. A couple of Holybro X500 6.1 equipped with Qorvo DWM1000 has been chosen as a test platform. These drones were mainly chosen due to the RTK GNSS system onboard, which is crucial for evaluating accuracy and is used as source of ground truth.

6.0.1 Line segment test

This experiment aims to test maximum range and get transfer characteristic of the sensor. The first UAV purpose was to act as an observer and for the entire duration of the test stayed at position $(0, 0, 0)$. Second UAV was flying in a trajectory predefined by parametric equation 6.1.

$$\text{position}(t) = \begin{pmatrix} 0 \\ 65 + 55 \sin(2\pi t) \\ 5 \end{pmatrix}, \quad t \in (0, 1) \quad (6.1)$$

6.0.2 Circular trajectory

As it was noted before, the results from UWB should be the same for all orientations. To test whether that is a correct assumption, 4 experiments have been conducted. In each test one UAV acted as an observer and stayed

¹<http://mrs.felk.cvut.cz/research/micro-aerial-vehicles>



Figure 6.1: Holybro X500 ¹.

stayed at position $(0, 0, 0)$. The second UAV followed a circle of radius 10 m around the first UAV. The difference between the 4 experiments was relative angle respective to velocity vector.

■ 6.0.3 Leader follower algorithm

To test the fusion of UVDAR and UWB in-loop, a leader-follower algorithm has been used. In this test, a leader UAV flies a preplanned trajectory. A follower UAV tries to follow the leader based only on UVDAR and UWB sensor fusion. The algorithm was inspired by [11].

■ 6.1 Results

All proposed experiments were successfully conducted. The first experiment [Figure 6.2] showed that the UWB measurements are indeed precise and do not express any signs of nonlinearity. The maximum range of 120 m was reached by UWB, however, the measurements at the far end are not reliable and often drops out. This can be seen as straight lines in Figure 6.2. Somehow cite this [2]

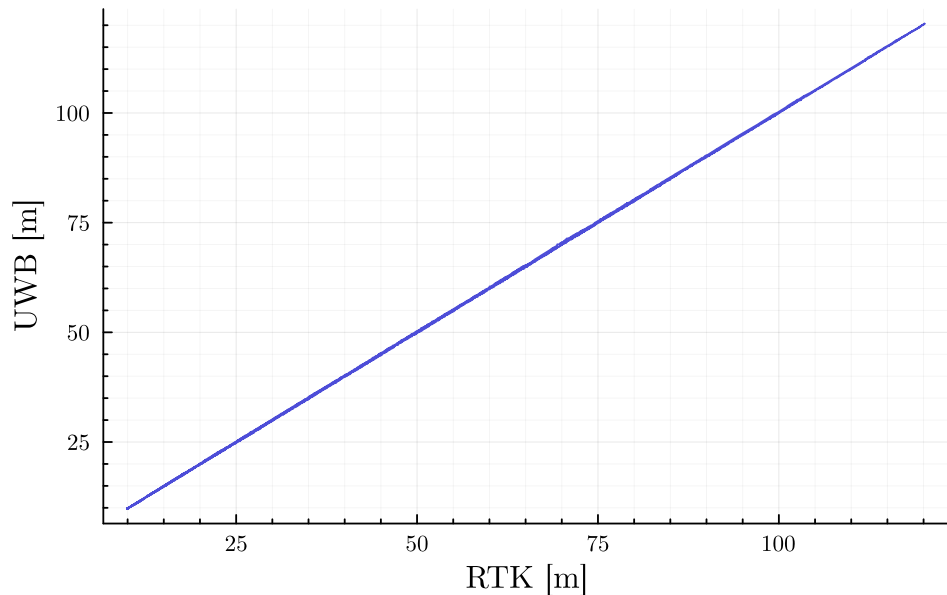


Figure 6.2: Transfer characteristic of UWB

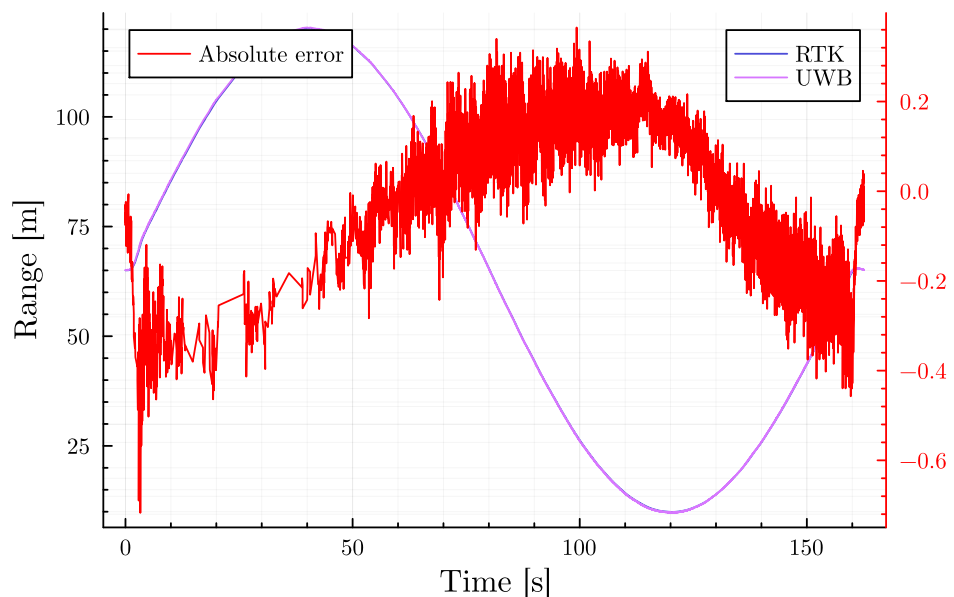


Figure 6.3: Transfer characteristic of UWB

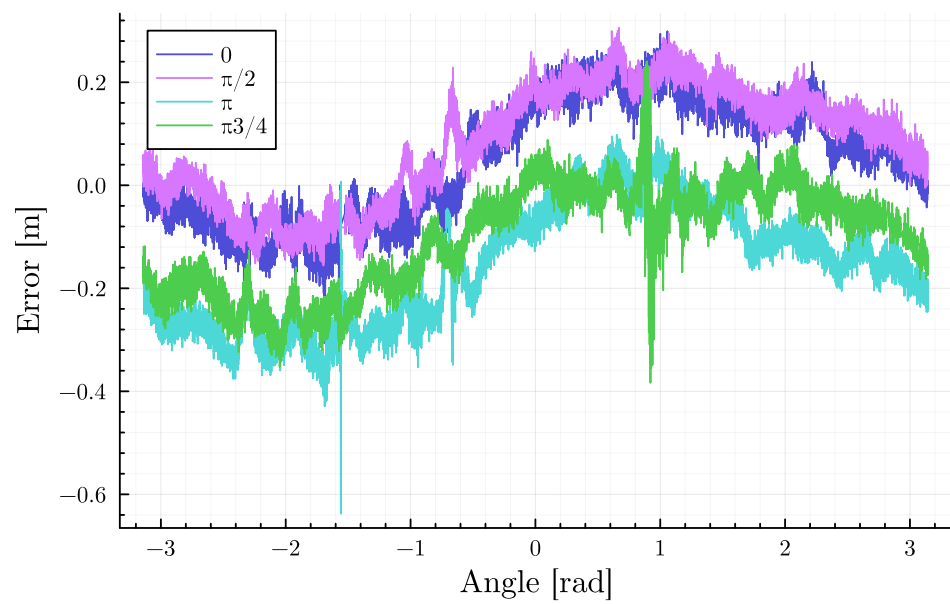


Figure 6.4: Transfer characteristic of UWB



Chapter 7

Conclusion

Bibliography

1. 2011. IEEE standard for local and metropolitan area networks—part 15.4: Low-rate wireless personal area networks (LR-WPANs). *IEEE Std 802.15.4-2011 (Revision of IEEE Std 802.15.4-2006)*: 1–314. <https://doi.org/10.1109/IEEESTD.2011.6012487>
2. 2014. *A sources of error in DW1000 based two-way ranging scheme APS011*. Decawave; <https://www.qorvo.com/products/d/da008446>.
3. 2016. IEEE standard for low-rate wireless networks. *IEEE Std 802.15.4-2015 (Revision of IEEE Std 802.15.4-2011)*: 1–709. <https://doi.org/10.1109/IEEESTD.2016.7460875>
4. R. E. Kalman. 1960. A New Approach to Linear Filtering and Prediction Problems. *Journal of Basic Engineering* 82, 1: 35–45. <https://doi.org/10.1115/1.3662552>
5. Priya Shree Madhukar and L. B. Prasad. 2020. State estimation using extended kalman filter and unscented kalman filter. In *2020 international conference on emerging trends in communication, control and computing (ICONC3)*, 1–4. <https://doi.org/10.1109/ICONC345789.2020.9117536>
6. MathWorks. 2021. Object tracking using time difference of arrival.
7. Rudolph Merwe and Eric Wan. 2003. Sigma-point kalman filters for probabilistic inference in dynamic state-space models. *Proceedings of the Workshop on Advances in Machine Learning*.
8. Matej Petrlik, Pavel Petracek, Vit Kratky, Tomas Musil, Yurii Stasinchuk, Matous Vrba, Tomas Baca, Daniel Hert, Martin Pecka, Tomas Svoboda, and Martin Saska. 2023. UAVs Beneath the Surface: Co-operative Autonomy for Subterranean Search and Rescue in DARPA SubT. *Field Robotics* 3: 1–68. <https://doi.org/10.55417/fr.2023001>

7. Conclusion

9. M. St-Pierre and D. Gingras. 2004. Comparison between the unscented kalman filter and the extended kalman filter for the position estimation module of an integrated navigation information system. In *IEEE intelligent vehicles symposium, 2004*, 831–835. <https://doi.org/10.1109/IVS.2004.1336492>
10. G. Vásárhelyi, Cs. Virág, G. Somorjai, N. Tarcai, T. Szörenyi, T. Nepusz, and T. Vicsek. 2014. Outdoor flocking and formation flight with autonomous aerial robots. In *2014 IEEE/RSJ international conference on intelligent robots and systems*, 3866–3873. <https://doi.org/10.1109/IROS.2014.6943105>
11. Viktor Walter, Nicolas Staub, Antonio Franchi, and Martin Saska. 2019. UVDAR system for visual relative localization with application to leader–follower formations of multirotor UAVs. *IEEE Robotics and Automation Letters* 4, 3: 2637–2644. <https://doi.org/10.1109/LRA.2019.2901683>
12. V. Walter, N. Staub, M. Saska, and A. Franchi. 2018. Mutual localization of UAVs based on blinking ultraviolet markers and 3D time-position hough transform. In *14th IEEE international conference on automation science and engineering (CASE 2018)*.
13. V. Walter, M. Saska, and A. Franchi. 2018. Fast mutual relative localization of uavs using ultraviolet led markers. In *2018 international conference on unmanned aircraft system (ICUAS 2018)*.
14. E. A. Wan and R. Van Der Merwe. 2000. The unscented kalman filter for nonlinear estimation. In *Proceedings of the IEEE 2000 adaptive systems for signal processing, communications, and control symposium (cat. no.00EX373)*, 153–158. <https://doi.org/10.1109/ASSPCC.2000.882463>
15. Yan Xie, Gerard J. M. Janssen, and Alle-Jan van der Veen. 2016. A practical clock synchronization algorithm for UWB positioning systems. In *2016 IEEE international conference on acoustics, speech and signal processing (ICASSP)*, 3891–3895. <https://doi.org/10.1109/ICASSP.2016.7472406>
16. Wenda Zhao, Abhishek Goudar, and Angela P. Schoellig. 2022. Finding the right place: Sensor placement for UWB time difference of arrival localization in cluttered indoor environments. *IEEE Robotics and Automation Letters* 7, 3: 6075–6082. <https://doi.org/10.1109/LRA.2022.3165181>